Quadratic Area Preserving Maps in $\mathbb{R}^2$ [1]

Carles Simó
Departament de Matemàtica Aplicada i Anàlisi
Universitat de Barcelona, Barcelona, Catalunya
carles@maia.ub.es

1 Introduction

We consider a map $F : \mathbb{R}^2 \to \mathbb{R}^2$ and we are interested in the behaviour of the iterates of the points in $\mathbb{R}^2$ (or in some open connected subset of $\mathbb{R}^2$). If $z_0 = (x_0, y_0) \in \mathbb{R}^2$ is some initial point, we want to see what is the behaviour of the iterates $z_{k+1} = F(z_k)$. The set $\{z_k, k \in \mathbb{N}\}$ is known as the orbit of z_0.

There are different ways to produce such a map, F. We can give it explicitly or we can consider an autonomous ordinary differential equation (ODE) $dz/dt = f(z)$ and define $F(z)$ as the image of a point z under the flow of the ODE after a fixed time τ: $F(z) = \varphi(\tau, z)$ or simply $\varphi_\tau(z)$, the so-called *time-τ map*.

Another interesting way to arrive at F is to use the so-called *Poincaré map*. Assume we have an ODE, $dw/dt = f(w)$ in $\mathbb{R}^3$ (or in some open connected subset of it or in a 3D manifold) and let Σ be a surface in $\mathbb{R}^3$ given, for instance, by $g(w) = 0$ assuming g to be a smooth function. If the flow of the ODE intersects Σ transversally (that is, $f(w)$ is not tangent to Σ at any of the points $w \in \Sigma$) we can do the following. Take an initial point, $w \in \Sigma$, and look for the solution $\varphi(t, w)$ of the ODE starting at w. If there exists some $t = t(w) > 0$ such that $\varphi(t(w), w) \in \Sigma$ while $\varphi(t, w) \notin \Sigma$ for $0 < t < t(w)$, we define this point as the image $\mathcal{P}(w)$ of w under the Poincaré map $\mathcal{P}$. This is a map defined on the 2D manifold Σ.

A very important case arises when the vector field f comes from a Hamiltonian with two degrees of freedom on a given level of the energy. A *Hamiltonian system* of equations with n degrees of freedom and Hamiltonian $H(q, p)$ has equations of the form

$$\frac{dq_i}{dt} = \frac{\partial H}{\partial p_i}, \quad \frac{dp_i}{dt} = -\frac{\partial H}{\partial q_i}, \quad i = 1, \dots, n \tag{1}$$

for $(q, p) \in \mathbb{R}^n \times \mathbb{R}^n$ (or in suitable manifolds) and it is immediately clear that $H(q, p)$ is preserved along the solutions of the ODE. The value of $H(q, p)$ is known as *the energy*. If $n = 2$ and we consider a given value of the energy, we have an ODE in 3D. If we can define a Poincaré map, as we did before, we again obtain a map on a 2D manifold, Σ.

In that case, the map $\mathcal{P}$ has an important property: *it preserves the area in* Σ. Hence, from now on we can simplify the presentation. We will consider $\mathbb{R}^2$ instead of a general surface Σ, we will denote the map simply as F and, furthermore, we will assume that it is area preserving. This implies that one has $\det(DF(z)) = 1$ for all $z \in \mathbb{R}^2$, where DF denotes the differential of F. For shortness we will denote Area Preserving Maps as *APM*.

The simplest case concerns maps F of degree 1. They are of the form $F(z) = Mz + b, b \in \mathbb{R}^2$, where M is a 2×2 matrix. If we skip the trivial cases with double eigenvalue equal to 1, it is always possible to assume $b = 0$ by shifting the origin. The eigenvalues of M can be of the form

1) $\exp(\pm \mathrm{i}\alpha)$, $\alpha \in (0, \pi)$, a case known as *elliptic*,

2) λ, λ^{-1}, $\lambda > 1$, a case known as *hyperbolic*,

3) 1 double, but M cannot be diagonalised, a case known as *shear*.

Two further cases can also appear with eigenvalues λ, λ^{-1}, $\lambda < -1$ (usually known as hyperbolic with reflection) and -1 double, again with M non-diagonalisable. They reduce to 2) and 3) above by composing with the central symmetry $-\mathrm{Id}$ or taking F^2 instead of F.

[1] Text of the talk delivered on September 25, 2013, as opening lecture at the Facultat de Matemàtiques, Universitat de Barcelona, Barcelona, Catalunya. See http://www.maia.ub.es/dsg/2013/ for related slides.

For the three cases above, after a change of coordinates, the matrix M can be reduced to one of the types:

$$\begin{pmatrix} \cos(\alpha) & -\sin(\alpha) \\ \sin(\alpha) & \cos(\alpha) \end{pmatrix}, \qquad \begin{pmatrix} \lambda & 0 \\ 0 & \lambda^{-1} \end{pmatrix}, \qquad \begin{pmatrix} 1 & 1 \\ 0 & 1 \end{pmatrix}. \tag{2}$$

In the elliptic case, the dynamics is essentially a rotation according to (2). All the points have bounded orbits, confined to ellipses. We note also that if α is of the form $\alpha = \frac{m}{n}2\pi$, $\frac{m}{n} \in \mathbb{Q}$, $(m,n) = 1$, then all the points are fixed under F^n, an extremely degenerate situation. That is, all the points are periodic with minimal period n. We recall that a point z is called *periodic with minimal period* $n > 1$ if $F^n(z) = z$ and $F^k(z) \neq z$ for $k = 1, 2, \ldots, n-1$.

In the hyperbolic case, the dynamics is of saddle type. Written as $F(x,y) = (\lambda x, \lambda^{-1} y)$, according to (2), all the points with $x_0 \neq 0$ escape to infinity, while the points with $x_0 = 0$ tend to the origin.

In the shear case, we can write the map as $F(x,y) = (x+y, y)$, as given by (2). All points with $y_0 \neq 0$ tend to infinity, while the points with $y_0 = 0$ are all fixed.

Figure 1 shows the three cases, with an initial point, labelled as 0, and the images labelled as 1, 2, 3, ... It is very important to note that in this linear case *all the iterates belong to curves* which are solutions of linear ODE which preserve the area. That is, ODE associated with a Hamiltonian which is quadratic. In fact there exists a Hamiltonian such that the map F coincides with the time-1 map of the Hamiltonian flow.

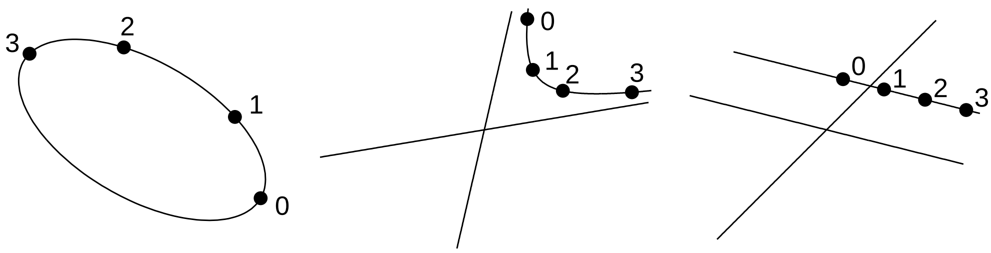

Figure 1: Examples of the dynamics of the three models of linear maps. From left to right: rotation, saddle and shear. The normal forms of the corresponding matrices are given in (2).

If for a general map F in $\mathbb{R}^2$ there exists a non-constant function G which is preserved by F, i.e., $G(F(z)) = G(z)$, we say that the map is *integrable*.

Hence, we pass to more interesting cases. The first that comes to mind is the case of *quadratic maps*. If we define $F(x,y) = (F_1(x,y), F_2(x,y))$ then F_1 and F_2 are quadratic polynomials in (x,y). This case is extremely relevant because

a) It allows for a reduction which decreases in a dramatic way the number of parameters involved in the map. Furthermore it has some relevant symmetries and a very simple geometric interpretation. This will be considered in Section 2.

b) It appears in a natural way as a very good approximation in some parts of $\mathbb{R}^2$ when we consider arbitrary APM. In particular when we study Poincaré maps of a Hamiltonian with 2 degrees of freedom.

c) It is a paradigmatic model. Many problems concerning: the existence of invariant curves diffeomorphic to $\mathbb{S}^1$ (Section 4); the role of invariant manifolds of hyperbolic fixed or periodic points and how they lead to the existence of chaos (Section 5); the geometrical mechanisms leading to the destruction of invariant curves (Section 6); and quantitative measures of different properties (Sections 7 and 8) for general APM [26], can all be understood thanks to our knowledge of the quadratic case.

Several questions still remain open, a few of which will be presented in Section 9.

Furthermore quadratic APM are *analytic*, a fact which allows us to apply useful results for analytic maps, and even more: they are *entire maps*. For a complete discussion of properties of different kinds of Hénon map and some applications, see [19]. Several of the figures and ideas presented here are taken from this paper.

2 Reduction and symmetries

At the end of the sixties, *Michel Hénon* [13] started the study of quadratic APM. Later on, on the middle of the seventies, he looked at the dissipative case [14]. In that case the Jacobian is constant but of absolute value below 1. It gives rise to the popular *Hénon attractor*.

However a remarkable fact, that is not difficult to prove, is that a constant Jacobian plus suitable shifts of the origin and scaling of variables, allow us to write any quadratic map in $\mathbb{R}^2$ in the form:

$$F:(x,y)\to(1-ax^2+y,bx) \tag{3}$$

for some constants a,b. When a tends to 0, scaling should be performed in a different way. Obviously the Jacobian is equal to $-b$ and, hence, the conservative case is obtained for $b=-1$.

The conservative map has a very simple geometric interpretation. It is the composition of two maps. The first one is $(x,y)\to(x,y+1-ax^2)$, one of the so-called *de Jonquières* maps, while the second is just a rotation by an angle of $-\pi/2$. Figure 2 shows, for $a=-1/2$, the square $[-3,3]^2$ (in red), the first image (in green) and part of the next two images (in blue and magenta, respectively). One can ask whether all points will escape for future iterations. As an answer to this question, we plot in black the set of points which remain bounded for all iterations and the selected value of a. This is the kind of objects we want to study together with how they change as a function of the parameter.

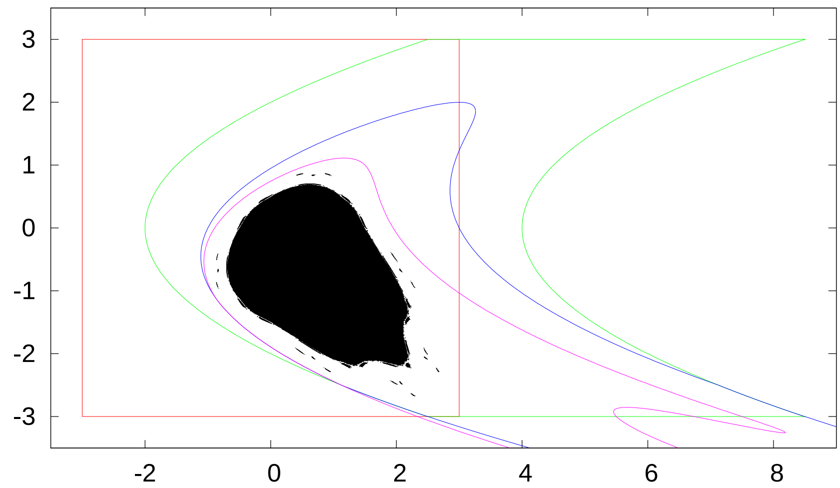

Figure 2: The square $[-3,3]^2$ (in red) and the first three images of it under the Hénon map with $a=-0.5, b=-1$, shown in green, blue and magenta, respectively. The last two have parts outside the frame shown here. The set in black displays the invariant set of points which remain bounded under all iterations.

A better representation of the quadratic APM, to be used in what follows, is:

$$F_c\begin{pmatrix} x \\ y \end{pmatrix}\to\begin{pmatrix} x+2y+\frac{c}{2}(1-(x+y)^2) \\ y+\frac{c}{2}(1-(x+y)^2) \end{pmatrix}, \tag{4}$$

where it is enough to consider $c>0$. It is obtained from a minimal modification of the version given in [34]. The subscript c in F_c is introduced to stress that the map depends on this parameter. The map has two fixed points. One of them is located at $(-1,0)$ and it is hyperbolic for all $c>0$. The other one, located at $(1,0)$, is elliptic for $0 < c < 2$, parabolic (concretely of shear type) for $c = 2$ and hyperbolic with reflection for $c > 2$.

It can immediately be checked that the inverse map can be expressed as $F_c^{-1} = SF_cS$, where S is the symmetry given by $S(x,y) = (x,-y)$. Hence, if we define $R = SF_c$, clearly an involution like S, we have $F_c = SR$ and $F_c^{-1} = RS$. Both S and R are called *reversors*. We can consider the sets of fixed points of both reversors, i.e., either points $z = (x,y)$ such that $S(z) = z$ (which are the points with $y = 0$) or points such that $R(z) = z$, which belong to a parabola.

There is an important property due to the existence of reversors of a map F. If K is a reversor and z^* is a point in the set $\mathrm{Fix}(K)$ of fixed points of K, then, if there exists $m \in \mathbb{N}$ such that $F^m(z^*) \in \mathrm{Fix}(K)$, the point z^* is periodic under F. Obviously, if $F^m(z^*) = z^*$, it has period m; and if $F^m(z^*) \neq z^*$, it has period $2m$. It is also clear that a fixed point can always be considered as periodic with period 1.

To study the local linear properties at a periodic point z^* with period m, it is enough to consider the linear map defined by $DF^m(z^*)$ and to use the description of the dynamics in Section 1. Accordingly, the point will be called elliptic, hyperbolic, hyperbolic with reflection or, if the eigenvalues of $DF^m(z^*)$ are $+1$ double or -1 double, parabolic.

3 A limit flow: comparison with the maps

A useful device for a preliminary study of the dynamics of a map F, provided it is *close to the identity map*, is to look for the existence of some ODE such that the time-1 map associated with the flow gives a good approximation to F. Looking at (4) suggests to introduce new variables $(\xi,\eta) = (x, 2y/\sqrt{c})$. Then, in the (ξ,η) variables, F_c differs from Id by $\mathcal{O}(\sqrt{c})$. A scaling of time also by $\sqrt{c}$ leads to:

$$\frac{d\xi}{dt} = \eta, \quad \frac{d\eta}{dt} = 1 - \xi^2, \tag{5}$$

an ODE which is Hamiltonian with $H(\xi,\eta) = \frac{1}{2}\eta^2 - \xi + \frac{1}{3}\xi^3$ (see (1)). So, the solutions are contained in the level curves of H. The dynamics of (5) is elementary and the main features are shown in Figure 3 left. It has also $(-1,0)$ and $(1,0)$ as fixed points, of hyperbolic and elliptic type respectively.

The level $H = 2/3$ of the hyperbolic fixed point contains two unbounded branches (the upper one is, in turn, a branch $W^{s,+}$ of the *stable manifold* of the fixed point, while the lower one is a branch $W^{u,-}$ of the *unstable manifold* of that point) and a bounded branch which bounds a domain in $\mathbb{R}^2$. This last branch is known as the *separatrix* and it is formed by the other two branches of the invariant manifolds, which turn out to coincide: $W^{s,-} = W^{u,+}$. All points not bounded by the separatrix escape to infinity, with the exception of $W^{s,+}$. The points inside the separatrix move in periodic orbits of the ODE around the elliptic fixed point. These orbits foliate the bounded domain.

The separatrix goes from $\xi = -1$ to $\xi = 2$ and the maximal value of $|\eta|$ is $\sqrt{8/3}$. It is given as the solution of (5) with initial data $(2,0)$ for $t = 0$. Furthermore we should comment that this solution is a limiting case of elliptic function which tends to $(-1,0)$ for $t \to \pm\infty$ and has a *singularity* at $t = \mathrm{i}\pi/\sqrt{2}$.

The periodic orbits around the fixed point located at $(1,0)$ have a period which tends to $\sqrt{2}\pi$ when they approach that point, and it tends to ∞ when they approach the separatrix. The period monotonically increases, as follows from simple properties of elliptic functions.

How does this compare to the behaviour of F_c for c small? An illustration is shown in the right part of Figure 3. It has been computed for $c = 0.2$ using initial points on the x-axis with values 1.01 (0.04) 1.93, and displaying 5,000 points in each orbit after a transient of 10^6 iterates.

The separatrices for the map look coincident, but they are not (see Section 5). The orbits displayed seem to be on *invariant curves*. Probably most of them are but, after some careful computations, one can check that there exists a tiny interval of initial points near $x = 1.7412624214$ where some orbits seem to be *chaotic*. Taking initial points on the opposite side of the elliptic fixed point, in the approximate range $[-0.08343, -0.08246]$, it is also clear that the orbits do not lie on invariant curves around the elliptic point.

What can lead to this misinterpretation of the right part of Figure 3 and what is the true dynamics will be discussed in Sections 4 to 6.

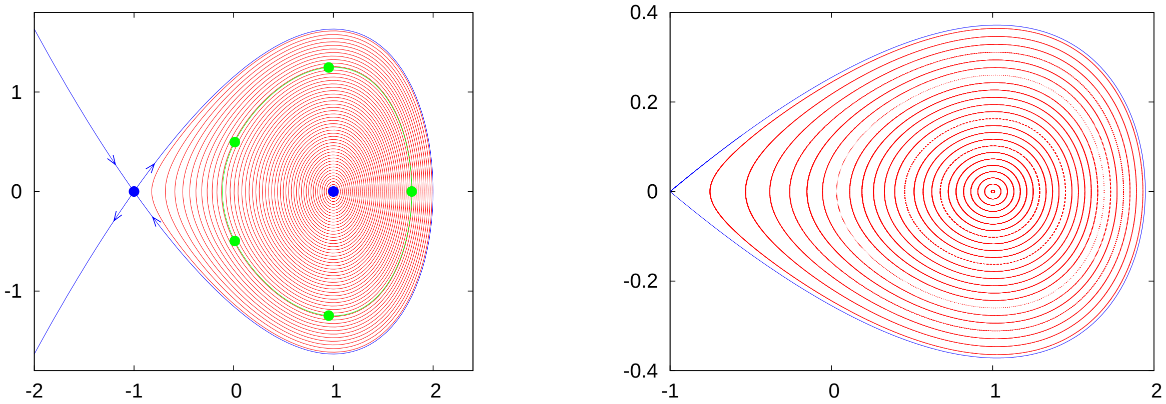

Figure 3: Left: the phase portrait of system (5). Fixed points are shown in blue, as are the invariant manifolds of the hyperbolic point. The periodic orbits are shown in red. See the text for details about the periodic orbit and the points shown in green. Right: the right branches of the invariant manifolds of the hyperbolic point and (part of) the orbits of several initial points under F_c, for $c = 0.2$.

An important characteristic of points whose orbit is an invariant curve is the *rotation number*. It measures the average value of the fraction of revolution that the point turns in each iterate. Looking at angles with respect to the elliptic fixed point (and in that case measured clockwise) not in $\mathbb{S}$ but on the lift $\mathbb{R}$, if the angle of the iterate k is denoted as θ_k the rotation number is defined as:

$$\rho = \frac{1}{2\pi} \lim_{k\to\infty} \frac{\theta_k}{k}. \tag{6}$$

It always exists and does not depend on the initial point on the curve. Of course, the value of ρ depends on the invariant curve. If these curves are parametrized by the point x where they intersect the x-axis to the right of the elliptic point, we can write $\rho = \rho(x)$. There are plenty of methods to compute ρ and most of them do not depend neither on the existence of a central point (like what we have described so far) nor on the dimension of the space where the map is defined. See [11, 12, 24].

In the case of the flow, we can define the associated time-1 map φ_1 as we do in Section 1. Then the rotation number is the inverse of the period. To see the good agreement between the left and right parts of Figure 3, Figure 4 shows the rotation number in both cases as a function of x for $x > 1$. The rotation number of the flow has been scaled to account for the time scaling and we have also applied a tiny correction to the value of the initial x to take into account the fact that the manifolds of the map F_c intersect the x-axis at a point slightly below 2.

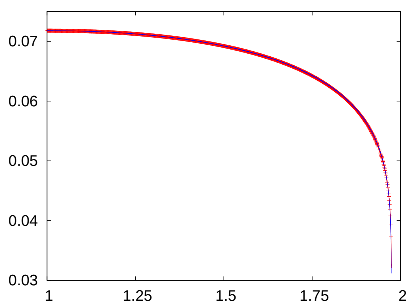

Figure 4: Comparison of ρ for the map $F_c, c = 0.2$, in red points, with the value for the field (5), as a blue line, after suitable scaling. Note the excellent agreement at this level of resolution.

Returning to the flow case, we have selected a point (the rightmost large point in green) on the left part of Figure 3 which defines a periodic orbit with period 5. So, this point has period 5 under φ_1; and it is clear that all the points in this periodic orbit of the flow have period 5 under φ_1. The other large points in green are the images of the rightmost one under $(\varphi_1)^k$ for $k = 1, 2, 3, 4$.

Hence, what would happen if we considered the map F_c, for c rather small, as a perturbation $\mathcal{O}(\sqrt{c})$ of the φ_1 map of the flow and we look for points with period n under iteration of F_c? The condition for an n-periodic point is $G(z) = F_c^n(z) - z = 0$. Writing $F_c^n = \varphi_1^n + \mathcal{O}(\sqrt{c})$, we may think of using the implicit function theorem to find solutions to $G(z) = 0$. But we would not succeed, because the differential of $\varphi_1^n - \mathrm{Id}$ is singular. Other means must be adopted.

More generally, we can ask if, given the map F_c, there exists an ODE (close to but different from the one in (5)) such that the associated φ_1 map coincides with F_c. We can even ask this in the case of arbitrary maps F, provided they (or some power of them in a suitable domain) are close to the identity map.

This turns out to be the case for APM F around a hyperbolic fixed point. The orbits under the φ_1 map of an ODE (which is shown to exist and is computable) coincide with those of F while they stay in a neighbourhood of the point. This is the content of the so-called Birkhoff Normal Form (BNF) see, e.g., [25]. Furthermore, in the case of the vicinity of an elliptic fixed point, a BNF can be computed to any order but, in general, it is *not convergent*. *Normal forms* are useful devices which provide a lot of information [1]. The key idea is to apply a sequence of transformations that convert the original problem into another which is easier to study.

If we are interested in the existence of an ODE whose φ_1 map coincides with a given close to the identity map F globally, that is, in a fixed compact domain K, there are also results based on averaging [20, 28]. To fix ideas we assume $F(z) = F_\varepsilon(z) = z + \varepsilon F_1(z, \varepsilon)$. The first step is to construct a *suspension*, that is, an ordinary differential equation depending periodically on time (e.g., with period 1) such that its time-1 map, from $t = 0$ to $t = 1$, coincides with the map F_ε [4]. This is always possible if ε is small. Then we apply a *sequence of transformations* with the aim of cancelling the time dependence of the ODE [20, 28]. In general this is not possible. The sequence of vector fields does not converge to an autonomous vector field. But stopping the process at the right place, which depends on ε, one can succeed in obtaining an autonomous vector field such that its time-1 map differs from the map $F_\varepsilon(z)$ by an amount bounded, for all $z \in K$, by $c_1 \exp(-c_2/\varepsilon)$ for some positive constants c_1 and c_2. See Section 5 for related topics, including the kind of divergence of the sequence of transformations.

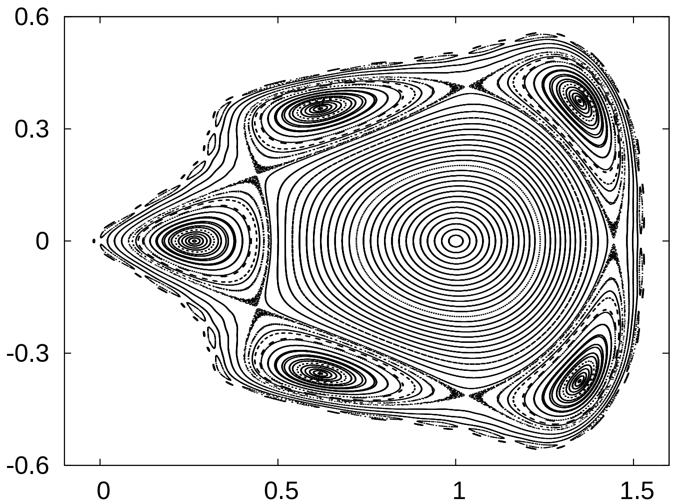

Figure 5: Some orbits under the map F_c for $c = 0.762$. As before, we take initial points and plot 5,000 iterates of each one after a transient of 10^6 iterates. Now the initial conditions on $y = 0$ are 0.98 (-0.02) -0.02. Points outside the domain displayed escape to infinity close to the branch W^{u-}.

Figure 5 illustrates what we find for larger values of c. Still, for a domain around the elliptic fixed point, it seems that there are many invariant curves. Far away there are some *islands* around periodic elliptic points of period 5. Close to the places where an island approaches its neighbours, it is possible to infer the existence of a periodic hyperbolic orbit of period 5. And in a vicinity of these periodic orbits the dynamics seems to be chaotic: the orbits seem to fill a set of positive measure, no longer confined to curves. Going to the periphery, one can find again more invariant curves surrounding the period-5 island

and, finally, some tiny chains of islands. This is the typical pattern that one finds for APM of any kind.

Note also that the islands of period 5 intersect $y = 0$ (i.e., the set $\mathrm{Fix}(S)$) on the left of the elliptic fixed point but not on the right, where one can guess a period-5 hyperbolic point. Other islands can intersect only to the right and some islands do not have intersection with $\mathrm{Fix}(S)$; but they can intersect $\mathrm{Fix}(R)$. To provide evidence of the existence of islands, in Figure 6 we plot the values of the rotation number as a function of x for initial points in $\mathrm{Fix}(S)$ (left plot) and also for initial points in $\mathrm{Fix}(R)$ (right plot) for $c = 0.7$. In the latter case we only use initial data to the left of $x = 1$. In both cases we observe that a maximum of ρ is achieved at $x = 1$. But, as we will see later, this can change with the value of c. In Figure 6, we mark with blue points the places where $\rho(x)$ is locally constant, which correspond to islands. In the places where there are nearby periodic hyperbolic points, the value of ρ is not defined, because of the lack of invariant curves and the existence of transversal homoclinic points (see Sections 5 and 6) and ρ has jumps.

The rotation number has been computed after a transient of 10^6 iterates using the next 10^6 and a method based on the order in which the iterates appear on the invariant curve. The values of x for which the iterates escape or are not located on invariant curves (this is automatically detected by the method) are skipped. The detected rational rotation numbers, using values of x of the form $k \times 10^{-3}, k \in \mathbb{Z}$, from left to right in the left plot, are 3/17, 25/141, 13/73, 7/39, 11/61, 15/83, 23/127, 2/11, 5/27, 1/5, 4/21, 2/11, 8/45, 14/79, 10/57 and 4/23: all with an odd denominator. In the right plot they are 1/6, 7/40, 13/74, 17/96, 11/62, 5/28, 9/50, 17/94, 29/160, 33/182 and 3/16: all with an even denominator.

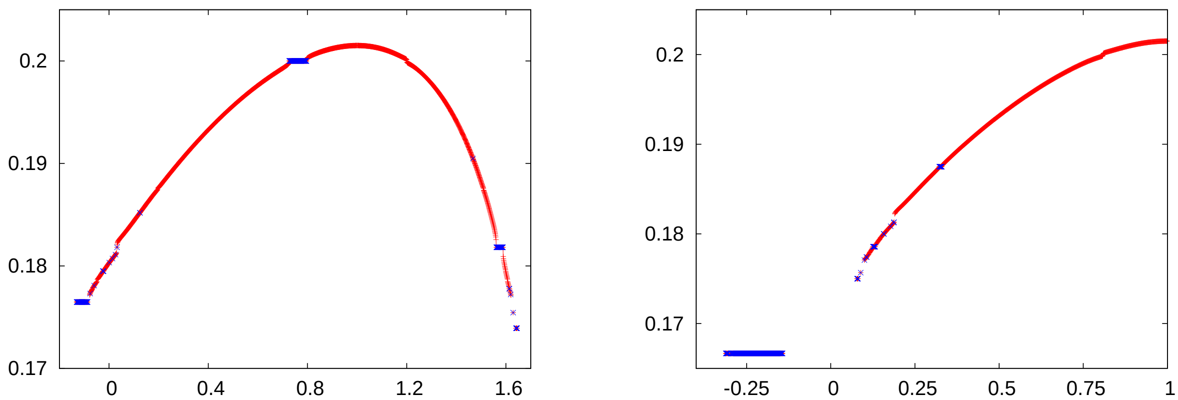

Figure 6: Rotation number as a function x for $F_c, c = 0.7$. Left: the initial points are taken on $y = 0$. Right: the initial points are taken on the set $\mathrm{Fix}(R)$, with the smallest value of y. Blue points denote places where the rotation number is rational and correspond to islands. See the text for details.

4 The existence of invariant curves

We are now interested in results ensuring the *existence of invariant curves*; not only for quadratic APM but for general APM. We will consider curves around an elliptic fixed point such that, taking polar coordinates centred at that point, the radius can be expressed as a function of the angle $r = r(\theta)$. Or simply curves defined on some *annular domain* but also having the property that the radius can be expressed as a function of the angle using a suitable central point.

First we introduce the so-called *twist maps*. These are *integrable maps* (hence they have a *foliation* by invariant curves in some annular domain). Assume that for $\theta = 0$, the radius r_0 varies in some domain $r_a < r_0 < r_b$ and we denote as $\rho(r_0)$ the corresponding rotation number. An APM of this type is said to satisfy the *twist condition* if $d\rho(r_0)/dr_0 \neq 0$. We will use the symbol T to denote such maps. Given an APM, suitable related twist maps can be obtained as time-1 maps of a flow which approximates the map (either around an elliptic fixed point, in an annulus or using some normal form).

Let us assume that the map in which we are interested is a *perturbation* of a twist map: $F_\varepsilon = T + \varepsilon P$, where P is a function normalised to have some norm equal to 1. By assumption, T has invariant curves. Can we ensure that they *subsist* for F_ε? The result is given by the so-called *Moser twist theorem*.

Theorem 4.1. *Consider a perturbation $F_\varepsilon = T + \varepsilon P$ of a twist map T. Then if we have an invariant curve of T which has Diophantine rotation number γ, this curve, with a small deformation, subsists for F_ε provided ε is sufficiently small.*

We need to introduce here a definition: *Diophantine number.* It is clear that any irrational number γ can be approximated as much as we want by rational numbers. The problem is that to have a good approximation we have to use rationals with *large denominators.* Hence, given a rational approximation $p/q, q > 0$ to γ we can measure how large the difference is compared to a power of $1/q$. Concretely, we say that γ satisfies a (C,τ)-*Diophantine condition* (for short (C,τ)-DC or simply DC) if $|\gamma - p/q| > C/q^\tau$ for some $C > 0$ and $\tau \geq 2$ and for all $p/q \in \mathbb{Q}$. It is easy to check that if we fix $\tau > 2$, the set of $\gamma \in \mathbb{R}$ which do not satisfy a (C,τ)-DC for any $C > 0$ has zero measure. Among the Diophantine numbers the best is the *golden ratio* $g = (\sqrt{5}-1)/2$. It satisfies DC for $\tau = 2$ (which is the minimal possible value of τ) and a maximal value of C which for rationals with denominator tending to ∞ tends to $1/\sqrt{5} \approx 0.4472136$. The worst value of C for g occurs when $p/q = 2/3$. Then $C = (9\sqrt{5}-21)/2 \approx 0.4376941$.

Hence, we have three conditions that guarantee that F_ε will have an invariant curve of the desired type:

a) It must be a *perturbation* of a twist map T,

b) The rotation number γ must be *Diophantine*,

c) It must be close enough to T, that is, ε must be *small.*

We can comment a little on the role of each one of these conditions. We start with the *Fourier representation* of the invariant curve of rotation number γ of T: $r(\theta) = \sum_{j\in\mathbb{Z}} a_j \exp(\mathrm{i}j\theta)$. Let $r_\varepsilon(\theta) = \sum_{j\in\mathbb{Z}} b_j \exp(\mathrm{i}j\theta)$ be the representation of the desired curve, invariant under F_ε. The *invariance condition* is expressed (in polar coordinates) as $F_\varepsilon(\theta, r_\varepsilon(\theta)) = (\theta + 2\pi\gamma, r_\varepsilon(\theta + 2\pi\gamma))$. It is clear that we can fix the origin of angles in an arbitrary way.

We try to pass from the coefficients a_j to the b_j by making a sequence of changes such that after the k-th change, one has an approximation of the invariant curve under F_ε with $\rho = \gamma$ with an error $\mathcal{O}(\varepsilon^{2^k})$. That is, a *Newton method* in the space of Fourier series. At each step one has to solve an equation which is of the form $G(\theta + 2\pi\gamma) - G(\theta) = R(\theta)$, the so called *homological equation*, where $R(\theta)$ is related to the error of the previous approximation and has *zero average*, a necessary condition in order to be possible to solve the equation.

Using Fourier representations for G and R: $G = \sum_{j\in\mathbb{Z}} g_j \exp(\mathrm{i}j\theta), R = \sum_{j\in\mathbb{Z}} r_j \exp(\mathrm{i}j\theta), r_0 = 0$, it is straightforward to obtain $g_j = r_j/(\exp(\mathrm{i}j2\pi\gamma) - 1), j \neq 0$. But, of course, if $j\gamma$ is close to an integer, the previous denominator is close to zero. This is known as the *small denominators problem.* The DC allows us to control the behaviour of the coefficients of G, so that if R is analytic in some complex strip around real values of θ, G is also analytic (perhaps in a slightly narrower strip).

The problem is then that the error in the next approximation *does not have zero average* and we will not be able to solve the next homological equation. But this average can be cancelled by modifying the initial independent term a_0 (or, equivalently, by selecting a proper value for g_0) and this is possible thanks to the twist condition. It is convenient to express the twist condition as $d\rho/da_0 \neq 0$; that is, in terms of the average of the initial curve. Finally the smallness of ε is necessary to have convergence in the Newton procedure. Note that, for a fixed γ, the larger the twist condition (say, $|d\rho/da_0|$), the larger the admissible values of ε are.

We also want to mention that the proof of existence of invariant curves for a given map and a given ρ can be made constructive, by producing rigorous bounds of the errors at the different steps using *Computer Assisted Proofs* (CAP).

Returning to the quadratic APM, it is instructive to compute rotation numbers for values of c and then for initial conditions either on Fix(S) ($y = 0$) or on Fix(R) to see where we can expect to find, respectively, *invariant curves, periodic islands, chaotic domains* or, simply, *escape.* This is shown in Figures 7 and 8. Note that most of the wedges associated with islands reach $x = 1$, but they are extremely narrow; below the pixel resolution. As rational numbers are dense, the red domains on these figures have, in fact, a *Cantor like structure.* There is a dense set of wedges to be removed from the red

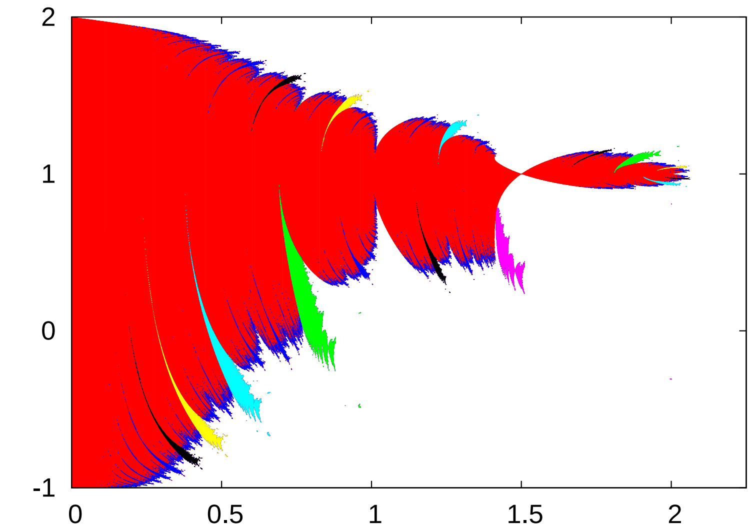

Figure 7: The plot shows, as a function of c, the values of x for points in $\mathrm{Fix}(S)$ for which the rotation number has been computed. The dots in red correspond to points for which $\rho \notin \mathbb{Q}$ while for the points in other colours $\rho \in \mathbb{Q}$. For $\rho = m/n$ and $n = 3, 5, 7, 9, 11$ the colours are magenta, green, pale blue, yellow and black, respectively. We use blue for other rational values.

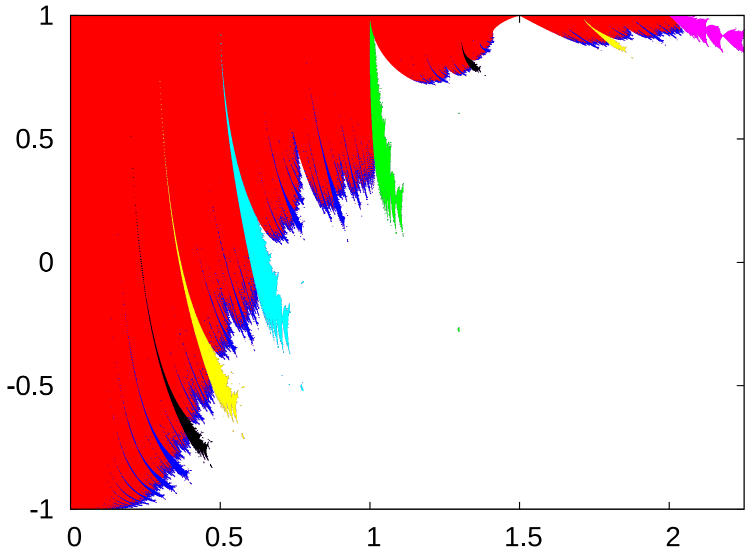

Figure 8: The plot shows, as a function of c, the values of x for points in $\mathrm{Fix}(R)$ for which the rotation number has been computed. The dots in red correspond to points for which $\rho \notin \mathbb{Q}$ while for the points in other colours $\rho \in \mathbb{Q}$. For $\rho = m/n$ and $n = 2, 4, 6, 8, 10$ the colours are magenta, green, pale blue, yellow and black, respectively. We use blue for other rational values.

domain, but this one has positive (and even relatively large) measure. This is related to the fact that the set of numbers satisfying a (C,τ)-DC for fixed $\tau > 2$ and very small C is a Cantor set with *almost full measure*.

We remark that some of the island domains in the previous figures do not emerge from $x = 1$. They are related to *satellites* (and satellites of satellites, and so on) of the main islands. In some sense, the structure around each island and around its satellite islands repeats the structure of the full set, as a *fractal object*.

At this point it is instructive to see how islands of a given rotation number evolve when c changes. The islands with rotation number p/q are born from $(1,0)$ at $c = 1 - \cos(2\pi p/q)$. To see their evolution we refer to *movie1* in `http://www.maia.ub.es/dsg/QuadraticAPM`.

A question arises in a natural way: what happens if the approximate integrable map *loses the twist property*? In Figure 9 we display the variation of ρ with x for $c = 1.35$. Comparing with Figure 6 we see, first, that in Figure 9 the value of ρ at $x = 1$ is a local minimum instead of a maximum. Then we see a maximum for $x < 1$ (those for $x > 1$ in both plots being related to that one). The twist condition is lost, but still some invariant curves can exist; see Figure 10. They are the so-called *meandering curves*, which cannot be written with the radius as a function of the angle seen from the elliptic point. The curves have some folds (or meanders) but there are tools to prove that they really exist [29].

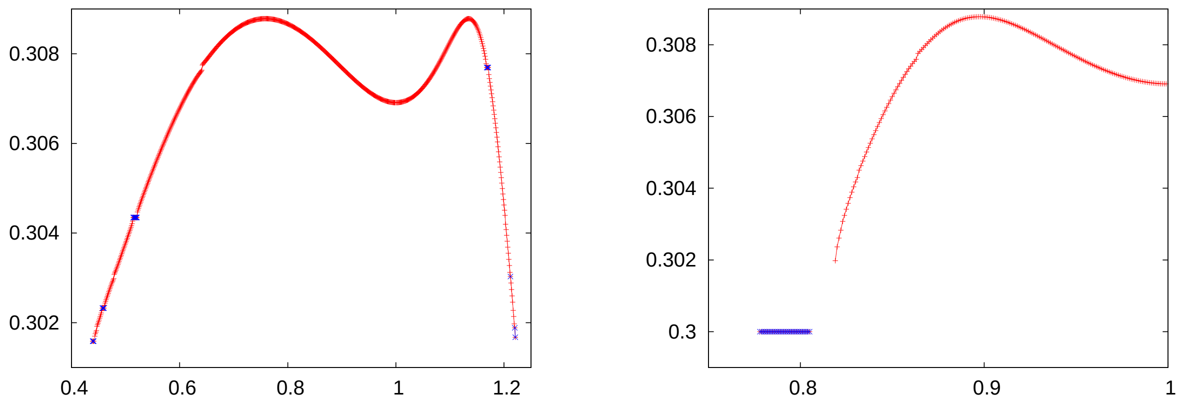

Figure 9: Similar to Figure 6 but for $c = 1.35$. The value of $\rho = \rho(x)$ is plotted for initial points on $y = 0$ (left) and on $\mathrm{Fix}(R)$ (right). In blue the points with $\rho \in \mathbb{Q}$. Note that now, to the left or to the right of $x = 1$ the function ρ is no longer monotonous.

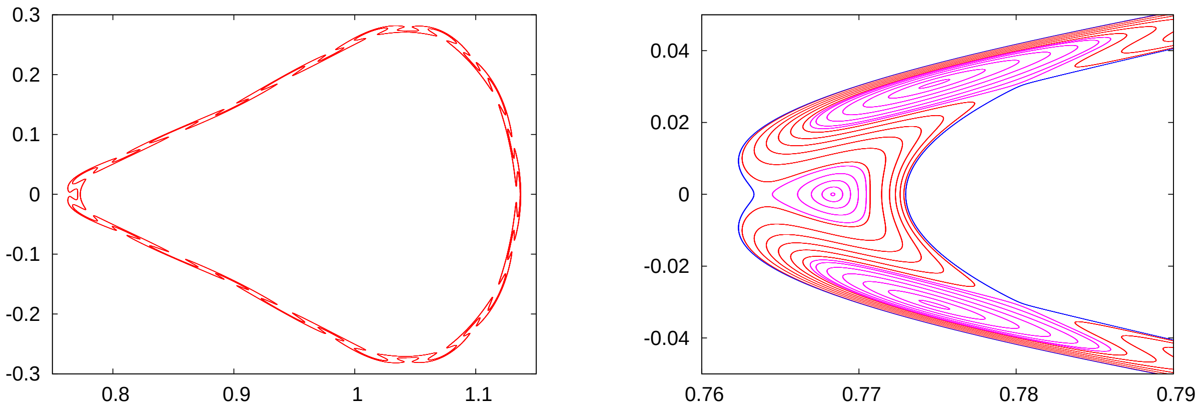

Figure 10: On the left we show a couple of orbits for $c = 1.3499$, sitting on a domain in which ρ passes through a maximum. These orbits are on invariant curves known as meanders. On the right we show a magnification. Beyond different meanders in red, one can see two ordinary invariant curves (inner and outer) in blue and islands which belong to two different chains of islands of rotation number $4/13$.

This kind of curves starts at $c = 5/4$ and lasts until $c \approx 1.4123$. The related rotation numbers range in the interval $I = (\cos^{-1}(-1/4)/(2\pi) \approx 0.29022, \approx 0.32846)$. They are related to the fact that two different chains of islands with the same rotation number coexist. For any rational $\rho \in I$ the same phenomenon appears, but in extremely narrow domains if ρ has a large denominator.

5 The invariant manifolds of hyperbolic points and their role in the creation of chaos

Beyond the invariant curves of an APM there are other very important invariant objects which play a key role in dynamics (this is also true for more general maps and flows in any dimension). They are the *stable and unstable manifolds of the hyperbolic fixed points* and can be seen as the non-linear generalisation of the invariant lines shown in the middle plot of Figure 1. A first example is shown in the right plot in Figure 3. We mentioned that in that Figure the branches $W^{u,+}$ and $W^{s,-}$ (the ones which start to the right of $x = -1$) seem to be coincident but they are not. In Figure 11, left, we reproduce these manifolds for $c = 0.2$ and in the right plot we show a magnification when they return to the vicinity of the point $(-1, 0)$, after going clockwise around $(1, 0)$ under F_c (red points) or counterclockwise under F_c^{-1} (blue points). We see tiny oscillations with a size $\mathcal{O}(10^{-3})$. Figure 12 shows similar manifolds for $c = 0.3$ and now the oscillations are some 10 times larger and one can guess them even in the left plot, very close to $(-1, 0)$. Similar objects appear if instead of fixed points we consider hyperbolic periodic orbits.

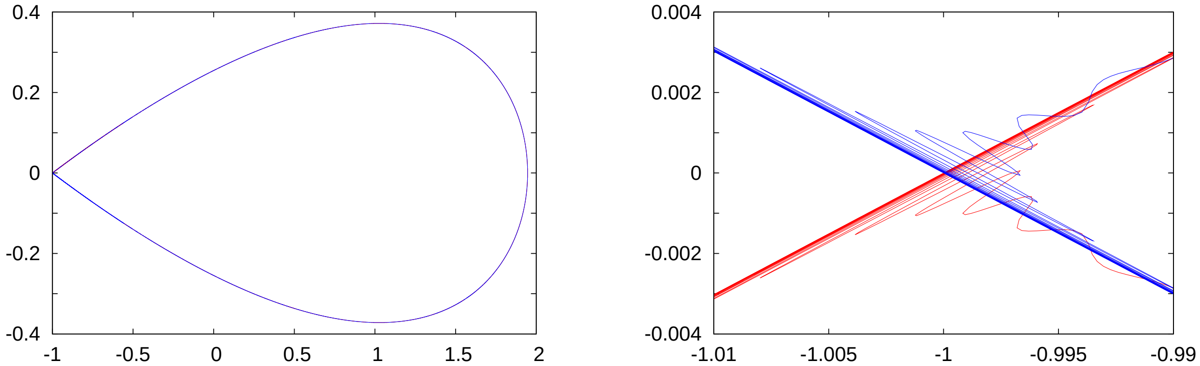

Figure 11: Invariant unstable (in red) and stable (in blue) manifolds of the hyperbolic fixed point for $c = 0.2$. The right plot is a magnification of the left one near the fixed point. In the left plot it seems that the manifolds coincide. The splitting is rather small.

They are called invariant because we ask that points on one of these curves (either W^u or W^s) should be mapped to points on the same curve under F and F^{-1}. Furthermore, the points on W^s tend to the hyperbolic fixed point or periodic orbit under iteration by F and the same thing happens for the points on W^u under iteration by F^{-1}. The invariance condition is also what allows us to obtain local expansions of these manifolds [27].

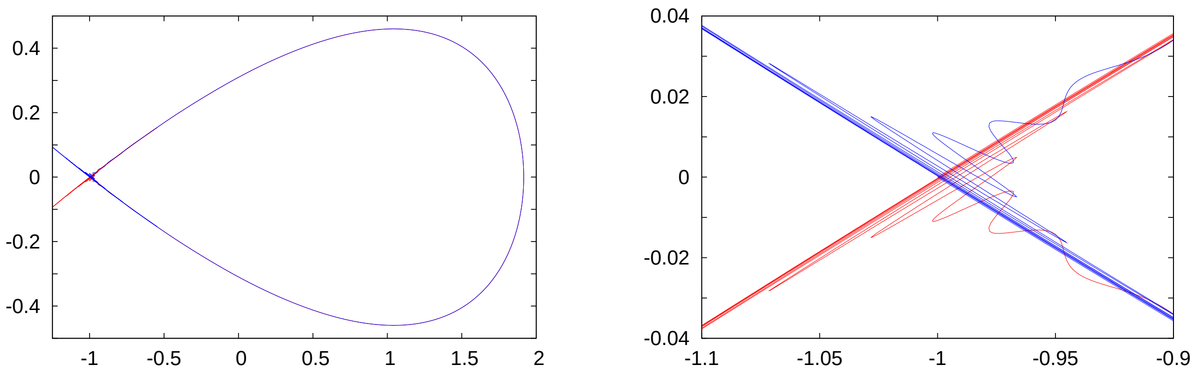

Figure 12: Similar to Figure 11 for $c = 0.3$. In the left plot one can start to see that the manifolds are slightly different. The splitting is small.

Why are they relevant? These manifolds have a *transversal intersection* when they cross the line $y = 0$ to the right, near $x = 2$. In fact, because of the existence of the reversor S, they satisfy $W^s = S(W^u)$. Points where a stable and an unstable manifold of a fixed or periodic hyperbolic point intersect are known as *homoclinic points*. It can also happen, as we will see in Section 6, that the unstable manifold of a (fixed or periodic hyperbolic) point Z_1 intersects the stable manifold of another (fixed or periodic hyperbolic) point Z_2. In that case, the intersection is known as a *heteroclinic point*. It is clear, because of the invariance, that if a point is homoclinic (respectively, heteroclinic), all the *images and preimages* under F are also homoclinic (respectively, heteroclinic).

When c increases, the lack of coincidence of W^u and W^s becomes more apparent. Figure 13 shows these manifolds for $c = 0.77, 1.0$ and 1.5.

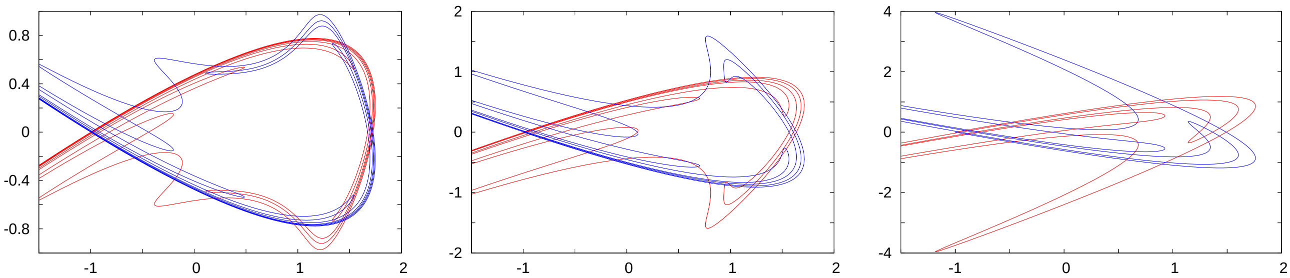

Figure 13: Similar to the left part in Figures 11 and 12 but for $c = 0.77, 1.0$ and 1.5, from left to right. The splitting of the manifolds is clearly visible and increasing. At the same time, note that the domain around the elliptic fixed point at $(1, 0)$ which is not covered by the oscillations of the manifolds, becomes smaller.

A measure of the lack of coincidence of the stable and unstable manifolds is the *splitting angle*. This is defined as the angle between them at a given homoclinic point. In the present case of quadratic APM, we can measure the angle at the *first intersection* of the manifolds with $y = 0$ to the right of $x = 1$ and see how it behaves as a function of c. For concreteness we denote this angle as $\sigma(c)$. In Figure 14, top, we represent the value of $\sigma(c)$ in different forms. In the left plot, despite the splitting is different from zero for any $c > 0$, we see that only for $c > 0.2$ does it start to be visible. To make what happens for small c visible, we display, in the top right plot, $\log(\sigma)$ against $\log(c)$. Note that already for $c = 0.05$ the value of $\sigma(c)$ is below 10^{-15} and, hence, *negligible for any practical application*.

Let $\lambda(c)$ be the dominant eigenvalue at the hyperbolic fixed point, which is equal to $1 + c + \sqrt{2c + c^2}$ for F_c. An essential parameter in the theoretical study of the problem is $h(c) = \log(\lambda(c))$, because using suitable representations of the manifolds, it is possible to show that the splitting has upper bounds of the form $\exp(-\eta/h)$, where η is related to the imaginary part of the singularity of the separatrix of the limit flow, as mentioned in Section 3. This type of result is true for *general analytic APM close to the identity map* [7, 8]. In fact, for the present problem one can prove a more precise result. The splitting angle has the form

$$\sigma(c) = \frac{9}{2} \times 10^6 \pi^2 h(c)^{-8} \exp\left(-\frac{2\pi^2}{h(c)}\right) \times \Omega(h). \tag{7}$$

The bottom left plot in Figure 14 illustrates the properties of (7). The variable on the horizontal axis is here $\log(h(c))$ while on the vertical axis we plot $\log(\sigma(c)) + 2\pi^2/h(c)$. According to (7), this should be (if we discard the $\mathcal{O}(h)$ term in the bound of $\Omega(h)$, see next paragraph) a line with a slope of -8, which agrees perfectly with the data. Note that the fact that we are computing rather small values of $\sigma(c)$ is not a problem at all. We have used a local representation of the manifold to order 400 and 500 decimal digits in the computations. The package PARI/GP [3] is useful for these simple problems.

The term $\Omega(h)$ can be expanded in powers of h^2: $\Omega(h) = \sum_{m\geq 0} \omega_{2m} h^{2m}$ and can be bounded by $\omega_0 + \mathcal{O}(h)$. The constant term can be determined numerically (see methods in [30, 10]) and the first digits of ω_0 are 2.48931280293671. Note, however, that the series defining $\Omega(h)$ is *divergent*; but for every value of h it provides a good approximation if we truncate the summation at the right place. There is

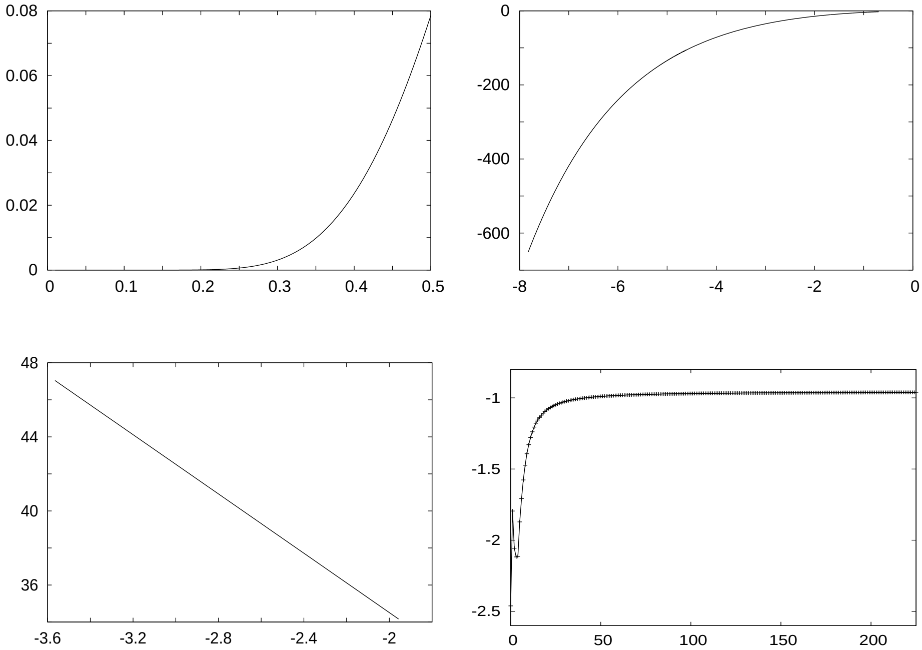

Figure 14: Top: Different representations of the splitting angle $\sigma(c)$ between the manifolds at the first intersection with $y = 0, x > 1$. Left: σ as a function of c, showing that σ seems negligible for $c < 0.2$. Right: $\log(\sigma)$ as a function of $\log(c)$, which allows to see how small $\sigma(c)$ is for c approaching zero. Bottom left: $\log(\sigma) + 2\pi^2/\log(\lambda(c))$ as a function of $\log(\log(\lambda(c)))$, showing an almost linear dependence with a slope of -8, in agreement with theory. Bottom right: the values of $\log_{10}(\omega_{2m}(2\pi^2)^{2m}/(2m+6)!)$ as a function of m, to give evidence of the Gevrey character of $\Omega(h)$.

numerical evidence that the series is of the *Gevrey-1 class*; that is, despite being divergent, the related series $\sum_{m\geq 0} \omega_m h^{2m}/(2m)!$ is convergent. The bottom right plot in Figure 14 shows this evidence. From a numerical determination of $\Omega(h)$, for different values of h, one can obtain the coefficients ω_{2m}. In the figure we plot $\log_{10}(\omega_{2m}(2\pi^2)^{2m}/(2m+6)!)$ as a function of m, which seems to tend to a constant.

This Gevrey character is also to be expected in *most of the formal constructions of flows* whose time-1 map approximates a given APM (or even general maps) close to the identity map.

To explain the *source of chaos* due to the existence of transversal homoclinic points, we return for a while to Figure 5. It is clear that between the period-5 islands there is an hyperbolic periodic orbit of period 5. Replacing F_c by F_c^5 the points on the periodic orbit become fixed points. If we look at one of the islands, for instance the leftmost one, and at the manifolds of the neighbouring fixed points, the structure is similar to the phase portrait of a *pendulum*, but now the separatrices *do not coincide*: the stable and unstable ones intersect transversally on the $y = 0$ axis. It can be shown that this situation is topologically equivalent to the *figure eight pattern* shown on the left of Figure 15 [35]. One can see tiny oscillations of the branches of W^u around W^s near p and vice versa. Note that the pattern shown in Figure 15, is not to be found in the Hénon map, but in other families, such as the *Duffing conservative map* or some representation of the *standard map*.

The right plot is a magnification of the left one. Consider two points such as A and B, close to $W^{u,+}$ but *on different sides* of $W^{s,+}$. They can be as close as we like. When, after several iterations, say m iterations and define $\Phi = F^m$, the points return near p as $\Phi(A)$ and $\Phi(B)$, as they are on different sides of $W^{s,+}$ in the subsequent iterates the point $\Phi(A)$ will move *to the right* and $\Phi(B)$ will move *to the left*. The system has *sensitive dependence to initial conditions*. This process repeats every time the iterates of a point return near to p. In fact, given an arbitrary bi-infinite sequence of symbols ℓ and r, such as $\{\ldots, \ell, \ell, r, r, r, \ell, r, \ell, r, \ldots\}$, one can show that there are points that realize that sequence in the successive passages near p. That is, the dynamics is *unpredictable*. The system is *deterministic* but it displays *chaotic dynamics*.

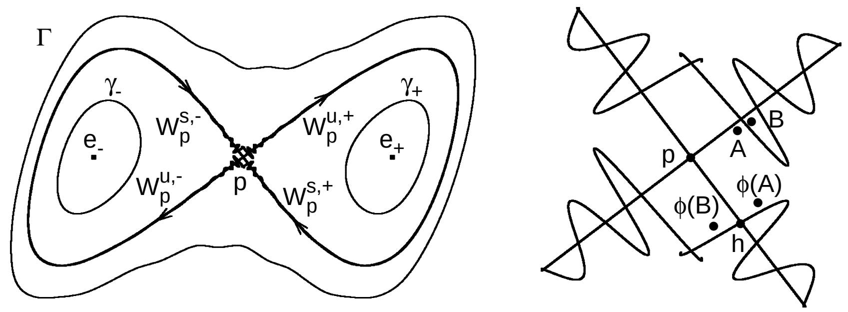

Figure 15: Left: an hyperbolic fixed point p whose invariant manifolds give rise to two loops (or a figure eight loop). Also shown: two elliptic fixed points, e_+ and e_-, together with invariant curves around them, γ_+ and γ_-, and an external invariant curve Γ. Right: a detail of the return of points A and B to the vicinity of p, as $\Phi(A)$ and $\Phi(B)$ useful to understand the origin of chaos. See the text for details.

6 The mechanism of destruction of invariant curves and the associated Cantor sets

As mentioned in Section 4, if the rotation number is too close to a rational (in the Diophantine sense) or if the twist condition is too weak or if the perturbation with respect to an integrable map is too large, the invariant curve *does not exist.* These analytic properties also have a nice *geometric interpretation* though. Before going into the details we can look at *movie2* in `http://www.maia.ub.es/dsg/QuadraticAPM`, which provides evidence of the *destruction of invariant curves*, around islands of period 6, 5 and 4, as c increases. Points in red in the images lie on invariant curves, while points in green have chaotic dynamics. Note that these last points are *confined* while there is an *invariant curve around them.* When this curve is destroyed, the points *escape* under iteration.

To illustrate the mechanism leading to the *destruction* of invariant curves we consider Figure 16. It has been produced for $c = 0.63$ and it shows the left part of the set of points which have bounded orbits. The case of Figure 16 is similar to the one in Figure 5, but now the main islands are 6-periodic. In black we display two chains of islands of rotation number 3/19 and 4/25. Consider the associated hyperbolic periodic orbits, that with rotation number 4/25 being visible on the x-axis and two symmetric points of the hyperbolic periodic orbit of rotation number 3/19 being close to $x = -0.2$ off the x-axis. The manifolds of these periodic orbits give rise to *heteroclinic connections*, as described in the caption.

These heteroclinic connections are *obstructions* to the existence of invariant curves which could separate the chains of islands. Indeed, if we consider a curve formed by a piece of invariant manifold of the inner hyperbolic periodic point (the one of period 25) until the heteroclinic point, followed by a piece of invariant manifold of the outer hyperbolic periodic point (the one of period 19), from the heteroclinic point to the periodic one, the invariant curves *will have to cross it.* This *is impossible because of the invariance.* In fact, one concludes that invariant curves with rotation number in the interval $(3/19, 4/25)$ cannot exist. But invariant curves with a rotation number in that interval are found for $c = 0.618$. Hence, the geometrical mechanism responsible for the destruction is the existence of heteroclinic connections which obstruct the possible curves [21, 23].

It is not necessary that a heteroclinic connection be transversal to forbid the existence of invariant curves. It is enough to have *tangential contact*, that is, the related unstable and stable manifolds are tangent. It is quite common that by changing parameters, two manifolds that were far away start to approach until they have a tangency and, after that, they become transversal, producing homoclinic or heteroclinic points. Some periodic orbits can be created *near the tangency* and, in particular, they can be of elliptic type, giving rise to periodic islands. Again, the model to understand the behaviour near the tangency is the Hénon map. Careful examination of that process reveals that, for analytic maps, homoclinic points already existed before the tangency, but they belong to the *complex phase space.* This amounts to considering the Hénon map (or other analytic maps) not in $\mathbb{R}^2$ but in $\mathbb{C}^2$. At the tangency, these points simply *land on the reals* [15].

As we will comment in Section 8, there are no invariant curves around the islands of period 6 already for a value $c \approx 0.6204$. In particular, the curves between the islands of period 19 and 25 in Figure 16 have

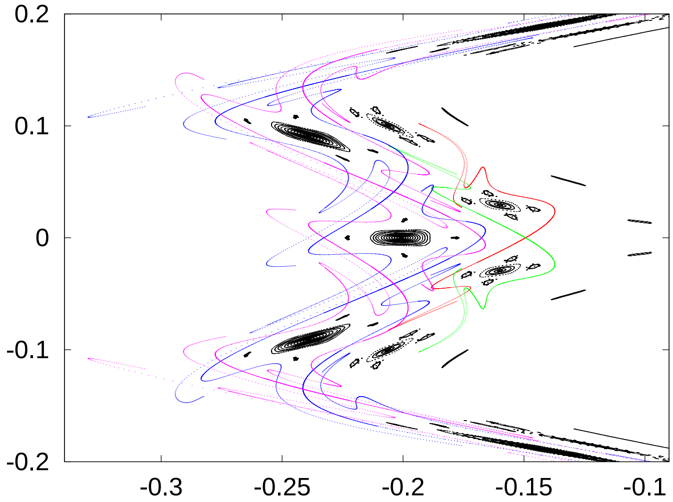

Figure 16: An illustration of the mechanism of destruction of invariant curves for $c = 0.63$. In black: part of two chains of islands of period 19 (the one which intersects $y = 0$) and 25. In red and green we show the unstable and stable manifolds W^u_{25}, W^s_{25}, respectively, of an hyperbolic periodic orbit of period 25. In blue and magenta the unstable and stable manifolds W^u_{19}, W^s_{19}, respectively, of a hyperbolic periodic orbit of period 19. Note that W^u_{25} and W^s_{19} (and, symmetrically W^s_{25} and W^u_{19}) have transversal heteroclinic points. This produces an obstruction to the existence of the invariant curves which could separate the chains of islands. See the text for details.

been destroyed. But we only start to see the heteroclinic connections in that figure for $c = 0.63$. Similar plots with $c = 0.625$ or $c = 0.628$, for instance, do not provide evidence of the existence of heteroclinics. The reasons of this are simple:

i) The arc length of the part of the manifolds in Figure 16 is short. If we plot similar parts of the manifolds for $c = 0.628$ the red manifold does not touch the magenta one, neither does the green manifold touch the blue one (because of the symmetry). But longer parts of the manifolds do intersect. In particular, there are arcs of the invariant manifolds which escape to infinity (under F_c for W^u and under F_c^{-1} for W^s).

ii) Between the chains of islands shown in Figure 16 there are many other periodic hyperbolic orbits (in fact, an infinity of them). So, it is possible to find a *chain of heteroclinic connections* between some of these orbits, which provides the desired obstruction. In turn this implies the existence of heteroclinic connections between the orbits of periods 19 and 25.

Anyway, there are invariant objects with rotation numbers in the above mentioned interval. It is proved that they should be *outside* the manifolds of the hyperbolic periodic orbit with $\rho = 4/25$ and *inside* the manifolds of the hyperbolic periodic orbit with $\rho = 3/19$. The heteroclinic intersections of these manifolds create *gaps* which *forbid the existence of points of the invariant object* in them. As a consequence, this object is a *Cantor set* [17, 18, 22] and is proved to have *zero measure*.

Therefore, the points with chaotic dynamics that were confined when the invariant curve still existed, can escape when the curve is destroyed and it is replaced by a Cantor set. If the gaps of that set are rather small, however, it will take a *long time* for the iterates to find their way to escape. This will be seen in Section 8.

7 Measuring the amount of chaos: Lyapunov exponents and entropy

To study the linear stability properties of a fixed point or a point in a periodic orbit of period k, say z^*, under a map F, one has simply to compute $DF(z^*)$ or $DF^k(z^*)$ and look for the eigenvalues, as described in Section 1. The question is how to proceed for *general orbits*, as we have in the case of points in invariant curves or with chaotic dynamics.

The basic idea is to use the *average of the exponential rate of increase of the distance* between the points of the orbit and those in an arbitrarily close orbit [5]. In general we can consider that the map F acts on a manifold Σ. Let $z \in \Sigma$ be an initial point and ξ a vector in the tangent space to Σ at z: $T_z\Sigma$. Furthermore, we assume ξ to have a norm equal to 1. Then we compute $DF^m(z)(\xi)$ and look at the rate of increase of the logarithm of the norm to define a number

$$\Lambda(z,\xi) = \lim_{m\to\infty} \frac{1}{m} \log |DF^m(z)(\xi)| \qquad (8)$$

known as the *Lyapunov exponent* at z in the direction of ξ. It has been proved that the limit exists for almost all $\xi \in T_z\Sigma$ and for almost all $z \in \Sigma$. The maximal value of $\Lambda(z,\xi)$ when ξ ranges in the unitary tangent bundle in $T_z\Sigma$ is known as *maximal Lyapunov exponent* at the point x: $\Lambda(z)$. For almost all $\xi \in T_z\Sigma$, one has convergence to $\Lambda(z)$.

To obtain an estimate of $\Lambda(z)$, one has to rescale the vectors $DF^m(z)(\xi)$ (otherwise the norm may increase too much) and use different devices to be confident regarding the estimate [31, 16]. For orbits in an invariant curve with irrational ρ (these orbits are obviously dense) the value of $\Lambda(z)$ is zero; while orbits with chaotic dynamics give, generically, positive values of $\Lambda(z)$. There are chaotic orbits which also produce $\Lambda(z) = 0$, but they are rather exceptional [9].

Returning to the quadratic APM F_c we have computed the maximal Lyapunov exponents for many values of c and a narrow grid of points. A typical spacing in the coordinates x and y for the grid is 0.0005. In most of the cases we first compute a transient of 10^6 iterates before starting to compute $\Lambda(z)$. In this way we detect most of the points which escape. A value $m = 10^6$ is also used in (8) to produce an estimate of $\Lambda(z)$. If the value obtained is below 2×10^{-5}, the orbit of z is considered to be regular. Otherwise it is considered to be chaotic. In the latter case, we continue with additional iterations (up to 10^8 and in some cases up to 10^{10}) to check if we can consider the chaos as confined or if the orbit of z finally escapes. Some results are shown in Section 8.

A global indication of the regular or chaotic properties of the system is given by the *metric entropy* $h_m(F)$. There are several equivalent ways to define it, but the simplest one to implement is the integral of the Lyapunov exponent in the set of bounded orbits, see [16]. It tells us how *chaotic* the map is *globally.*

8 Changes in the measure of the set of non-escaping points

The plot showing the *measure* $\mu(c)$ of the set of *bounded orbits* as a function of c for the map F_c, as given in (4) is quite instructive. We should stress that there are many other more general conservative models (e.g., Hamiltonian systems with 2 or 3 degrees of freedom, such as the Restricted Three-Body Problem, or travelling waves of some PDE, such as the Michelson system [32, 6]) which have *many features in common* with what we display for the Hénon conservative map.

Furthermore, for APM in a 2D manifold, every time that a homoclinic tangency is produced (i.e., for some fixed or periodic orbit, W^u and W^s have a tangency) a local study near the tangency shows maps quite similar to the Hénon one with similar global properties, as already mentioned in Section 6.

Figure 17 shows the measure $\mu(c)$ of the set of bounded orbits as a function of c and a magnification. Note the sudden decrease of the measure at some values of c. Going from right to left one can see a first decrease near $c = 1.5$. At that value of the parameter the elliptic point has eigenvalues $-1/2 \pm \mathrm{i}\sqrt{3}/2$ and it is (weakly) unstable. *No invariant curves exist around it.* The small confined area for $c = 1.5$ is due to the existence of tiny period-3 islands. Later on we see a sequence of sudden changes in $\mu(c)$ which correspond to the destruction of all the invariant curves surrounding the islands of periods 4, 5, 6 and so on.

The magnification shown in the right part of Figure 17 provides strong evidence of what happens with islands with a higher period and displays the self similar properties of $\mu(c)$. As an example, the large jump near $c = 0.91$ corresponds to the breakdown of invariant curves around the islands of rotation number 2/9 (compare this with the upper yellow domain in Figure 7); while the jump shortly after $c = 0.96$ corresponds to the breakdown of invariant curves around the islands of rotation number 3/13.

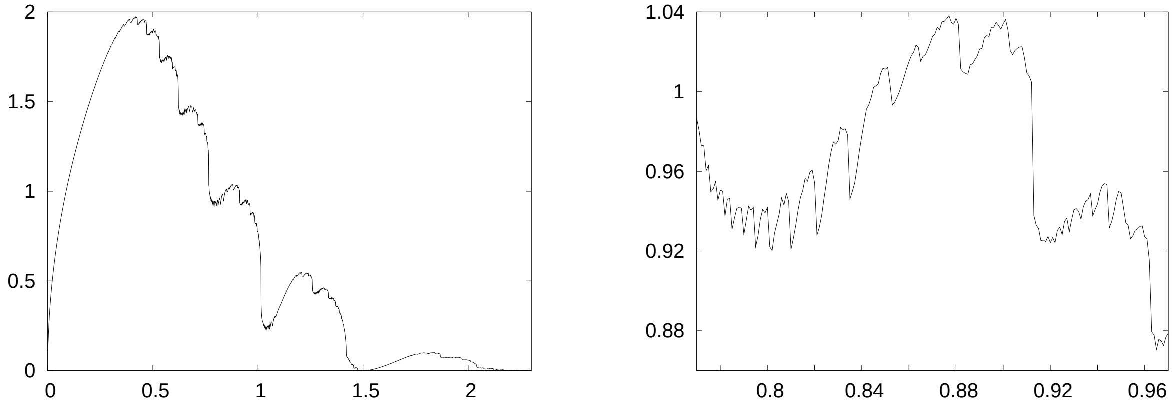

Figure 17: Left: measure $\mu(c)$ of the set of confined points as a function of c. Right: a magnification in the range $c \in [0.77, 0.97]$ to provide evidence of the self similar properties of this measure.

It is not difficult to identify all the jumps shown in these plots. As there are jumps in $\mu(c)$ for every slight change of c, one has evidence that it is a totally discontinuous function.

One can look at *movie3* in `http://www.maia.ub.es/dsg/QuadraticAPM` to see the changes not only concerning the *measure* but also the *shape* of the set of bounded orbits.

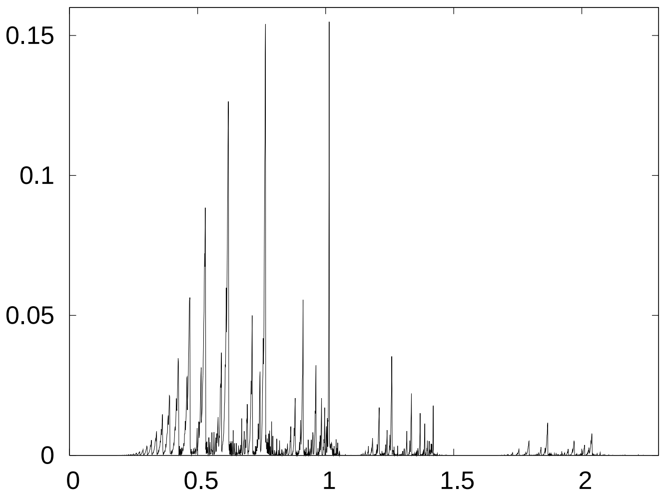

Figure 18: Measure of the set of confined points with chaotic dynamics as a function of c.

Among the points with bounded orbit there are, however, some which display chaotic behaviour. The Lyapunov exponent allows us to detect them. A natural question is, hence, how the measure of this set changes with the value of c. This is shown in Figure 18. The plot shows quite a sharp change in behaviour. This is to be expected, because of the infinitely many chains of islands in the system (there are for any $\rho \in \mathbb{Q} \cap (0, 1/2]$). Each chain of islands has an associated hyperbolic periodic orbit which generates some amount of chaos. It is confined until the invariant curves that surround these chaotic orbits breakdown. Even considering that the computations shown in Figure 18 have been done with a 10^{-3} step in c, a careful examination of the data allows us to detect several hundreds of picks.

On Figure 19, we show three magnifications. They correspond to what happens before the breakdown of the invariant curves around the islands of periods 6, 5 and 4, respectively. For the moment, we do not consider the small jumps on these curves; just a kind of average. For the left plot, this is produced by the change in the size of the chaotic zone created by the homoclinic points associated to the period-6 hyperbolic orbit. But this orbit has been created at $c = 0.5$. Hence, why does it take so long to see that the size of this zone is relevant? The answer is similar to the discussion we give in Section 5 concerning the change in the size of the splitting angle $\sigma(c)$ as a function of c. We also refer to the plots in Figure 14, specially the top left plot.

There, we realized that from the beginning of the existence of a non-zero splitting angle until it starts to be visible, the required change in c was, at least, equal to 0.2. In Figure 19, left, the situation is similar. Even if the splitting of the manifolds of the period-6 orbits starts at $c = 0.5$, it is only at a value of c close to 0.6 when it becomes visible. For the middle and right plots in Figure 19 the situation is quite similar. We want to remark only that the period-5 hyperbolic orbit has been created at $c = 1 - \cos(2\pi/5) \approx 0.690983$ and the one of period 4 has been created at $c = 1$. So, in these two cases the evolution of the splitting with c is faster.

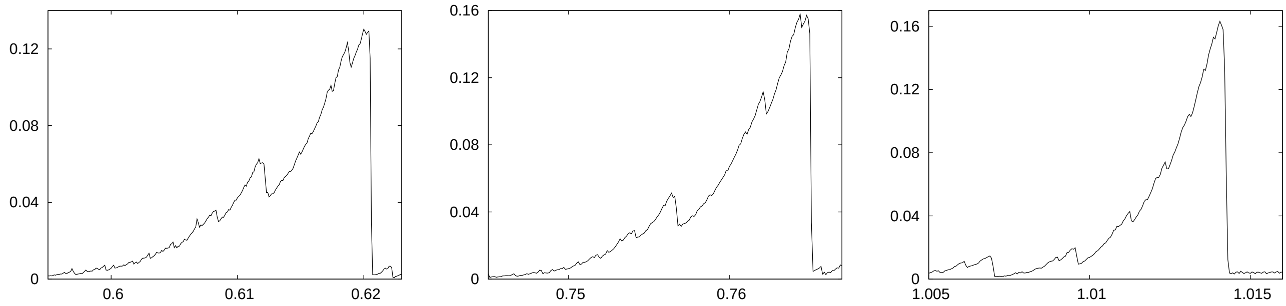

Figure 19: Magnification of Figure 18 corresponding to the breakdown of the invariant curves which surround the islands of period 6 (left), period 5 (middle) and period 4 (right).

The jump seen in the left plot shortly after $c = 0.61$ corresponds exactly to the same kind of phenomenon, created by the periodic orbit of rotation number $\rho = 3/19$. The measure of the chaotic zone associated with this periodic orbit has to be added, in some sense, to the largest chaotic zone due to the period-6 orbit.

We also mention that in the domain where one has evidence of the existence of chaos, tiny islands can be found. A proof of that fact using analytical/geometrical arguments can be found in [33].

Another point we want to illustrate is *how fast* the points in a chaotic zone escape when the surrounding invariant curves are broken, as a function of c. Let $c_{p/q}$ be the *critical value* at which the invariant curves surrounding the islands of rotation number $\rho = p/q$ breakdown. Then, when $c > c_{p/q}$, the points in the associated chaotic zone can escape. But is is clear that if $\Delta c = c - c_{p/q}$ is small, the gaps in the Cantor sets surrounding the chaotic zone are *narrow* and a *large number of iterates* will be needed, on average, to produce the escape.

Figure 20 shows examples along these lines. Approximate critical values for the periodic orbits related to the figure are $c_{1/6} \approx 0.6204, c_{1/5} \approx 0.7649$ and $c_{1/4} \approx 1.0141$. Let us discuss, for instance, the left plot. For a value such as $c = 0.625$, the fraction of points which remains after 10^5 iterates is relatively larger than that after 10^6 iterates. According to the figure, some 8% larger (green curve). If we look for the ones which remain after 10^6 iterates compared to the ones which remain after 10^7 iterates, the excess is approximately 1% (red curve). Finally, the measure of the points which remain after 10^7 iterates compared to those which remain after 10^8 iterates is almost negligible (blue curve). This means that a large part of the points in *chaotic non-confined orbits*, already escaped after 10^6 iterates and very few require 10^8 iterates.

The values change when we look at different values of c. For a value such as $c = 0.63$, most of the points already escaped after 10^5 iterates, while for $c = 0.621$, almost no points escaped before 10^7 iterates and most of them require 10^8 iterates or more.

If we go back to Figure 17 or 18, we should see that the jumps are instantaneous: either surrounding invariant curves exist and no escape is possible or they do not exist and all the points in the related chaotic zone should escape. But the simulations are performed with a finite number of iterations (as we said, ranging from 10^8 to 10^{10}, depending on the figure). The results shown in the middle and right plots in Figure 20, for different periods, are quite similar. The same behaviour has to be expected in most cases.

9 Some open problems

What is known at present about the dynamics of quadratic APM and also of more general APM allows quite a complete understanding of the different types of behaviour, the geometrical mechanisms and

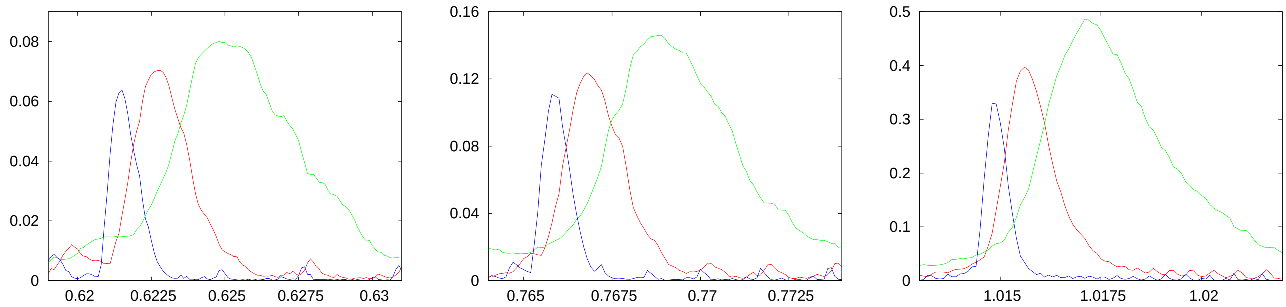

Figure 20: From left to right we plot results for the escape of points after destruction of the confining curves around the islands of period 6, 5 and 4, respectively. If M_n denotes the measure of the set of points with chaotic dynamics which have not yet escaped after n iterates, the curves in green, red and blue display the relative excess $M_{10^5}/M_{10^6}-1, M_{10^6}/M_{10^7}-1$ and $M_{10^7}/M_{10^8}-1$, respectively.

analytical estimates.

Still there are some classic problems which *remain open*. We can mention here a few of them. One should mention that they are *far from elementary* and have resisted many attempts up to now.

a) The quadratic APM are a special case of the so-called *Cremona maps*. These are polynomial maps in any dimension: $z \to T(z) \in \mathbb{R}^m$, where all the m components of T are polynomial with maximal degree n. Assume that the Jacobian of T is constant: $\det(DT(z)) = a$, $\forall z \in \mathbb{R}^m$ with $a \neq 0$ a real number. It is not restrictive to assume $a = 1$, otherwise we compose T with a suitable linear map. The so-called *Jacobian conjecture* asks: Is it true that the inverse map T^{-1} is also a polynomial map? The degree of T^{-1} need not to be the same as the degree of T.

   We know the answer is *yes* for quadratic Cremona maps and the inverse is also quadratic. This follows from the format of (4) and from the existence of the reversor S for quadratic APM which implies that the inverse of F_c is conjugated to F_c.

   This conjecture has been proved for degree two and there are results which reduce the problem to prove it in any dimension for polynomials of degree 3. Some results are also available for other special cases, but the general problem remains open.

b) We have seen that periodic orbits play a relevant role in the organisation of the dynamics of quadratic APM and this is also true for general APM.

   An old conjecture due to *Poincaré* asks: Consider the set of bounded orbits of an APM; is it true that the periodic orbits are dense in that set?

c) We have been talking in Sections 7 and 8 about the measure of the set of points with positive Lyapunov exponent; also about the metric entropy, as integral of the maximal Lyapunov exponent. But despite all numerical evidence there is a basic question which is still open.

   This is known as the *metric entropy conjecture*: Is the metric entropy of a non-integrable APM strictly positive?

   An equivalent question can be phrased as follows. Consider the stable or the unstable invariant manifold of a fixed or periodic point z^*. Is the Lebesgue measure of the closure of that manifold strictly positive?

d) In Section 4 we commented on Diophantine numbers and the *optimal* properties of the golden ratio g. The (C,τ)-DC can also be written as $|q\gamma - p| > C/q^{\tau-1}$ for all $(p,q) \in \mathbb{Z}^2, q \neq 0$.

   Let us pass to a *higher dimension*. Let $n > 1$ and $\omega = (\omega_1, \ldots, \omega_n) \in \mathbb{R}^n$. We say that the vector ω satisfies a (C,τ)-DC if $|\sum_{i=1}^n \omega_i k_i - k_0| > C/(||k||_2)^{\tau-1}$, for all $k = (k_1, \ldots, k_n) \in \mathbb{Z}^n$ where $||k||_2$ is the Euclidean norm, assumed to be positive, and all $k_0 \in \mathbb{Z}$.

   For a given $n > 1$, which is the *optimal* vector, in the same sense as we used for g?

Another quite general problem appears in the outlook in next section.

10 Conclusion and outlook

Quadratic Area Preserving Maps, despite appearing to be the first extension to be considered after the linear case, show an *extremely rich dynamics.*

Analytic, geometric and topological tools allow us to have a *fair understanding of the dynamics* and to find explanations for (almost) all facts observed numerically.

Still some points require a combination of analytical and numerical tools, like how to predict when different invariant curves will breakdown or how to predict statistical properties in the large.

Furthermore, the study of the quadratic case can be seen as a *paradigm* to be used to describe the properties of more general APM.

A key question is what happens when we *increase the dimension.* A natural generalisation of APM to manifolds of even dimension (say, dimension $2n$) are the *symplectic maps.* Assume that we use local coordinates $(x_1, x_2, \ldots, x_n, y_1, y_2, \ldots, y_n)$ and consider the 2-form $\omega = dx_1 \wedge dy_1 + dx_2 \wedge dy_2 + \ldots + dx_n \wedge dy_n$. A symplectic map is a transformation which preserves ω. It is clear that if $n = 1$ the form is nothing else than the area element. These transformations appear in a natural way as Poincaré maps for Hamiltonian systems with $n + 1$ degrees of freedom.

What can be said about the dynamics of symplectic maps? There are many partial results, like the existence of n-dimensional invariant tori (which generalise the invariant curves that we find in APM). Similar results are proved for Hamiltonian systems close to an integrable system, a topic studied by the *KAM theory* (see, e.g., [2]). The last open problem above is related to the properties of the *more persistent* invariant torus. But even for the case $n = 2$, a good description of the global properties of the dynamics is not yet available. This could be a nice research topic for the coming years.

Acknowledgements

The author's research has been supported through the years by European, Spanish and Catalan grants. He is also extremely indebted to multiple collaborators who contributed greatly to clarifying topics. And, in particular, to N. Miguel and A. Viero with whom the author is working on the same area. The computing facilities of the Dynamical Systems Group at the Universitat de Barcelona have been used for the numerical illustrations presented in these notes. Thanks also to the efficient work of J. Timoneda as system manager of the cluster.

References

[1] V. I. Arnold, Les méthodes mathématiques de la mécanique classique. Éditions Mir, Moscow, 1976.

[2] V. I. Arnold, A. Avez, Problèmes ergodiques de la mécanique classique. Gauthier-Villars, Paris 1967.

[3] C. Batut, K. Belabas, D. Bernardi, H. Cohen, M. Olivier, *Users' guide to PARI/GP*, `http://pari.math.u-bordeaux.fr/`

[4] H. Broer, R. Roussarie, C. Simó, Invariant circles in the Bogdanov-Takens bifurcation for diffeomorphisms. *Ergod. Th. & Dynam. Sys.* **16** (1996) 1147–1172.

[5] P. M. Cincotta, C. M. Giordano, C. Simó, Phase space structure of multidimensional systems by means of the Mean Exponential Growth factor of Nearby Orbits. *Physica D* **182** (2003) 151–178.

[6] F. Dumortier, S. Ibáñez, H. Kokubu, C. Simó, About the unfolding of a Hopf-zero singularity, *Discrete and Continuous Dynamical Systems – Series A*, **33** (2013) 4435–4471.

[7] E. Fontich, C. Simó, Invariant Manifolds for Near Identity Differentiable Maps and Splitting of Separatrices. *Ergod. Th. & Dynam. Sys.* **10** (1990) 319–346.

[8] E. Fontich, C. Simó, The Splitting of Separatrices for Analytic Diffeomorphisms. *Ergod. Th. & Dynam. Sys.* **10** (1990) 295–318.

[9] L. Garrido, C. Simó, Some ideas about strange attractors. In *Proceed. Sitges Conference on Dynamical Systems and Chaos*, *Lect. Notes in Physics* 179:1–28, Springer, 1983.

[10] V. Gelfreich, C. Simó, High-precision computations of divergent asymptotic series and homoclinic phenomena. *Discrete and Continuous Dynamical Systems B* **10** (2008) 511–536.

[11] G. Gómez, J.M. Mondelo, C. Simó, A Collocation Method for the Numerical Fourier Analysis of Quasi–periodic Functions. I: Numerical Tests and Examples. *Discrete and Continuous Dynamical Systems B* **14** (2010) 41–74.

[12] G. Gómez, J.M. Mondelo, C. Simó, A Collocation Method for the Numerical Fourier Analysis of Quasi–periodic Functions. II: Analytical error estimates. *Discrete and Continuous Dynamical Systems B* **14** (2010) 75–109.

[13] M. Hénon, Numerical study of quadratic area-preserving mappings. *Quart. Appl. Math.* **27** (1969) 291–312.

[14] M. Hénon, A two-dimensional mapping with a strange attractor. *Comm. Math. Phys.* **50** (1976) 69–77.

[15] V. F. Lazutkin, C. Simó, Homoclinic orbits in the complex domain. *Int. J. on Bifurcation and Chaos* **7** (1997) 253–274.

[16] F. Ledrappier, M. Shub, C. Simó, A. Wilkinson, Random versus deterministic exponents in a rich family of diffeomorphisms. *J. Stat Phys.* **113** (2003) 85–149.

[17] J. Mather, Minimal measures. *Comment. Math. Helv.* **64** (1989) 375–394.

[18] J. Mather, Action minimizing invariant measures for positive definite Lagrangian systems. *Math. Z.* **207** (1991) 169–207.

[19] N. Miguel, C. Simó, A. Vieiro, From the Hénon conservative map to the Chirikov standard map for large parameter values, to appear in *Regular and Chaotic Dynamics*, 2013.

[20] A. Neishtadt, The separation of motions in systems with rapidly rotating phase. *J. Appl. Math. Mech.* **48** (1984) 133–139.

[21] A. Olvera, C. Simó, An obstruction method for the destruction of invariant curves. *Physica D* **26** (1987) 181–192.

[22] A. Olvera, C. Simó, The dynamics near invariant Cantorian sets of perturbed twist maps. In *Synergetics, order and chaos*, M. G. Velarde, editor, pp. 698–705, World Scientific, 1988.

[23] A. Olvera, C. Simó, Elliptic non-Birkhoff periodic orbits in the twist maps. *Int. J. on Bifurcation and Chaos* **3** (1993) 165–185.

[24] J. Sánchez, M. Net, C. Simó, Computation of invariant tori by Newton-Krylov methods in large-scale dissipative systems. *Physica D* **239** (2010) 123–133.

[25] C. L. Siegel, J. K. Moser, Lectures on celestial mechanics. Die Grundlehren der mathematischen Wissenschaften, Band 187. Springer-Verlag, New York-Heidelberg, 1971.

[26] C. Simó, An overall view on conservative maps in the plane. In *European Conference on Iteration Theory (ECIT 87)*, C. Alsina et al., editors, pp. 56–73, World Scientific, Singapore, 1989.

[27] C. Simó, Analytical and numerical computation of invariant manifolds. In *Modern methods in celestial mechanics*, D. Benest and C. Froeschlé, ed., pp. 285–330, Editions Frontières, 1990.

[28] C. Simó, Averaging under fast quasiperiodic forcing. In Proceedings of the NATO-ARW *Integrable and chaotic behaviour in Hamiltonian Systems, Torun, Poland, 1993*, I. Seimenis, editor, pp. 13–34, Plenum Pub. Co., New York, 1994.

[29] C. Simó, Invariant Curves of Perturbations of Non Twist Integrable Area Preserving Maps. *Regular and Chaotic Dynamics* **3** (1998) 180–195.

[30] C. Simó, Analytic and numeric computations of exponentially small phenomena. In Proceedings *EQUADIFF 99*, Berlin, B. Fiedler, K. Gröger and J. Sprekels, editors, pp. 967–976, World Scientific, Singapore 2000.

[31] C. Simó, Global Dynamics and Fast Indicators. In *Global Analysis of Dynamical Systems*, H. W. Broer, B. Krauskopf, G. Vegter, editors, pp. 373–390, IOP Publishing, Bristol, 2001.

[32] C. Simó, Some properties of the global behaviour of conservative low dimensional systems. In *Foundations of Computational Mathematics: Hong Kong 2008*, F. Cucker et al. editors, pp. 163–189, London Math. Soc. Lecture Notes Series **363**, Cambridge Univ. Press, 2009.

[33] C. Simó, D. Treschev, Stability islands in the vicinity of separatrices of near-integrable symplectic maps. *Discrete and Continuous Dynamical Systems B* **10** (2008) 681–698.

[34] C. Simó, A. Vieiro, Resonant zones, inner and outer splittings in generic and low order resonances of Area Preserving Maps. *Nonlinearity* **22** (2009) 1191–1245.

[35] C. Simó, A. Vieiro, Dynamics in chaotic zones of area preserving maps: close to separatrix and global instability zones. *Physica D* **240** (2011), 732–753.